Phase diagrams of a model diluted fcc magnet with arbitrary spin and modified RKKY interaction: Influence of external magnetic field and structural short-range order

Karol Szałowski* and Tadeusz Balcerzak
Department of Solid State Physics, University of Łódź, ulica Pomorska 149/153, 90-236 Łódź, Poland
(Received 10 December 2007; revised manuscript received 31 January 2008; published 11 March 2008)

A diluted fcc magnet with modified long-range Ruderman–Kittel–Kasuya–Yosida interaction and arbitrary Ising spin S is considered within a two-sublattice model. The exponential damping for the long-range interaction as well as the nearest-neighbor antiferromagnetic superexchange couplings are taken into account. In the molecular field approximation, the Gibbs free energy is derived, from which all magnetic thermodynamic properties can be self-consistently obtained. In particular, the phase diagrams are studied for different magnetic ion and free charge carrier concentrations, taking into account the atomic short-range-order (Warren–Cowley) parameter and the external magnetic field. The stability regions of paramagnetic, ferromagnetic, and three characteristic antiferromagnetic phases are discussed. Moreover, the critical temperature and degree of magnetic frustration are evaluated to be dependent on the short-range order.

DOI: 10.1103/PhysRevB.77.115204 PACS number(s): 75.50.Pp, 75.10.−b, 75.30.Hx, 75.30.Kz

I. INTRODUCTION

The magnetic systems, the behavior of which is governed by the long-range interactions oscillatory in sign, inspire numerous theoretical efforts. The most representative example is the Ruderman–Kittel–Kasuya–Yosida (RKKY) interaction, in which the indirect coupling of the localized magnetic moments is mediated via free carriers, i.e., the electrons or holes. This mechanism is traditionally associated with spin-glass models and magnetic ordering in rare-earth metals (see, for example, Refs. 1 and 2). In the past a decade, a novel motivation for studying such systems has arisen owing to the discovery of diluted magnetic semiconductors (DMSs), which is important from the spintronics point of view.[3] The mechanism based on coupling mediated by charge carriers was suggested as an explanation for ferromagnetism observed in these substances.[4]

It may be useful to recall very briefly that magnetism in a celebrated DMS, $Ga_{1-x}Mn_xAs$, is an effect of the existence of spin-5/2 localized magnetic moments introduced by the substitutional Mn ions, which at the same time serve as acceptors. As a consequence, the holes of spin 3/2 appear for a low dopant concentration residing in a distinct impurity band which tends to merge with a valence band with increasing Mn content (for a recent review, see Ref. 5). This is reflected by the insulator to metal transition, in the progress of which the bound holes become delocalized. These carriers are responsible for the exchange interaction between impurity moments, the phenomenon which yields ferromagnetic ordering in some range of parameters. The extensive review can be found in Ref. 6.

A wide interest in studies of DMS is stimulating for investigations of the prototype models for these systems. One of the fruitful approaches is based on the RKKY interaction. In comparison with its ordinary form, several modifications have been proposed to sketch out the situation in DMS. First of all, the structural disorder, introduced by the random impurity spins, induces localization of the free carriers.[7,8] The influence of this localization on the long-range RKKY interaction can be conveniently described by the exponential damping factor,[9] which contains the characteristic length scale connected with the mean free path of the carriers. Another feature which should be taken into account is the existence of the short-ranged superexchange interaction between magnetic ions. This interaction, being antiferromagnetic in character, exists in addition to the long-range oscillatory couplings[10] and softens the ferromagnetic indirect interactions.

The conventional RKKY-based model along with the modifications described above has been discussed in the context of DMS properties[11–16] and has been subjected to extensive Monte Carlo (MC) studies[17] aimed at determining the phase diagram[13] as well as the critical temperatures[11,12] for the Heisenberg model. The results when compared directly with experimental data for $Ga_{1-x}Mn_xAs$ (Refs. 11 and 12) show reasonable agreement. The above mentioned study[13] supports the existence of the ferromagnetic ground state for this model by means of MC simulations albeit it covers only a limited range of charge carrier concentration, focusing on the regime upon which the number of carriers per single impurity spin was greatly reduced.

On the other hand, the vital importance of disorder itself in the description of DMS has recently been emphasized by numerous theoretical works (for a topical review, see Ref. 18 and references therein) and stimulated by the experimental data showing the great sensitivity of the critical temperature and magnetic ordering in $Ga_{1-x}Mn_xAs$ samples to their thermal treatment even though the concentration of magnetic impurities remains unchanged.[19] This suggests that the occupation of the lattice sites by magnetic ions may not be completely random.

For the case of $Ga_{1-x}Mn_xAs$, the effects of magnetic impurity clustering on the critical temperature of a model DMS have been extensively investigated. A recent general study of the influence of correlated disorder on the DMS properties was performed by Meilikhov,[20] who pointed out that ion clustering shifts the ferromagnetism stability range toward lower impurity concentrations and has the same effect on the position of the Curie temperature maximum. On the other hand, by means of the MC method, Priour and Das Sarma[14]

found only a weak influence of magnetic ion aggregation on the phase transition. In contrast, Bouzerar *et al.*[21] predicted a noticeable increase in Curie temperature of the clustered impurities system for $Ga_{1-x}Mn_xAs$ and $Ga_{1-x}Mn_xN$. The presence of clustering in DMS has been supported theoretically, for example, by the first-principles calculations of various alloy characteristics performed by Drchal *et al.*,[22] Kudrnovský *et al.*,[23] and Raebiger *et al.*[24] Also Berciu and Bhatt[25] studied the dependence of the Curie temperature on the distribution of magnetic dopants, with the outcome that the truly random positions elevate the critical temperature relative to the case of ordered ones. On the other hand, numerous existing works use different approaches to the clustering in order to show that it decreases the critical temperature in Ga-based DMS.[26–28] The various cluster configurations were also the subject of first-principles calculations[29] or density-functional studies.[30]

Obviously, exploring the behavior of three-dimensional diluted magnetically frustrated systems driven by the long-range oscillatory interactions constitutes a challenging task, even if limited to the ground-state properties. The full studies usually rely on the extensive use of simulations. Various variants of *ab initio* methods, yielding the crystalline, electronic, and magnetic structures, are believed to provide reliable estimations of critical temperatures for specific substances (for example, see Ref. 31). In such a situation, however, the identification of the influence of selected model parameters on the overall result requires significant numerical workload. Here, we see the importance of simplified, schematic models which could be extensively analyzed, providing some detailed insight, for instance, into the general features of the influence of the disorder on the magnetic properties.

It is also worth mentioning that in the range of very small dilution, the MC simulations do not detect the possible antiferromagnetic phases which, in principle, can be expected on the fcc lattice.[32–34] Moreover, the existence of the three characteristic antiferromagnetic phases, in addition to the ferromagnetic one, has already been found in the case of the pure RKKY interaction.[35] For the present model, with the important modifications of the interaction, i.e., with the damping, as well as with the nearest-neighbor (NN) antiferromagnetic superexchange couplings, the existence of all these phases needs to be reconsidered. It would also be interesting to explore the properties of the model not only for strong dilution, but also in some wider concentration range.

Second, the behavior of the model under the influence of an external field should be studied from the very beginning. As far as we know, the external field is seldom taken into account together with the RKKY interaction because the physical situation then becomes more complex. In such a case, not only the localized spins but also the spins of the carriers are influenced by the field, which leads to the additional polarization of both interacting subsystems. However, as it has been recently shown,[36] the influence of the external field can be conveniently introduced into the RKKY Hamiltonian by means of the effective gyromagnetic factor appearing in the Zeeman-like term. Such an improvement makes it possible to study the nonzero field phase diagrams, including all the modifications of the RKKY interaction discussed above.

We select an Ising-like Hamiltonian for our model system. Such a choice has the advantage of enabling one to obtain the exact ground-state results (in the numerical meaning, since no analytic formulas could be derived for the phase boundaries) without resorting to Monte Carlo methods. In this way, the importance of specific parameters becomes more transparent. We are convinced that the model reflects some of the essential ingredients of the physical situation in DMS, sketched out by the modified RKKY interaction we use. However, at the cost of simplifying the physical picture, we do not expect our model to provide any complete or accurate description directly comparable with the experimental data for a particular material.

Our aim is thus to analyze a model of a diluted magnet with modified RKKY interaction, focusing on the importance of external magnetic field and structural correlations in the distribution of magnetic moments on the lattice. We improve the virtual crystal approximation by taking into consideration the correlations of pairs, and we study its effect on the magnetic ground-state phase diagrams as well as the critical temperature. Moreover, we introduce a measure of magnetic frustration and discuss its sensitivity to structural correlations.

The paper is organized as follows: In Sec. II, the theoretical model is described in detail by a statistical-thermodynamical method. In particular, the analytical expressions for the Gibbs energy (in external magnetic field) and the phase transition temperature are derived. On this basis, the numerical calculations are carried out in Sec. III and the results are extensively presented in the figures. A recently developed approach[37] of numerical summation over an arbitrary large number of coordination zones is adopted. The discussion of the results in Sec. III is focused on the influence of configurational short-range order and external magnetic field on the magnetic phase diagrams. Moreover, the issue of magnetic frustration is addressed. Finally, in Sec. IV, some conclusions are drawn. The Appendix contains a method of configurational averaging in the pair approximation.

II. THEORETICAL MODEL

We consider the Ising-type Hamiltonian on the diluted fcc lattice containing an antiferromagnetic NN interaction as well as the long-range indirect interaction of the RKKY kind. In order to describe various antiferromagnetic structures, a model of two interpenetrating sublattices (a,b) is adopted. The Hamiltonian can be written in the following form:

$$\mathcal{H} = -\sum_{\langle i,j\rangle} J_{ij}\xi_i\xi_j S_i^a S_j^a - \sum_{\langle i,j\rangle} J_{ij}\xi_i\xi_j S_i^b S_j^b - \sum_{\langle i,j\rangle} J_{ij}\xi_i\xi_j S_i^a S_j^b - h\sum_i \xi_i S_i^a - h\sum_i \xi_i S_i^b, \tag{1}$$

where $S_i^\alpha = -S, \ldots, +S$ is the Ising spin of arbitrary magnitude S situated in ith lattice site and belonging to the sublattice α $(\alpha = a,b)$. In Eq. (1), $h = -g^{\mathrm{eff}}\mu_B H^z$ corresponds to the external magnetic field H^z oriented in the z direction, whereas $g^{\mathrm{eff}} = g_S + g_c m^* A k_F / 4\pi^2\hbar^2$ is the effective gyromag-

netic factor, which for the case of RKKY interaction has been introduced in Ref. 36. In the above formula, g_S and g_c are the gyromagnetic factors of the localized spin and the free carrier, respectively. m^* is the carrier effective mass, A is the contact potential between localized spin and the free carrier, and k_F is the Fermi wave vector. The effective gyromagnetic factor of a localized spin g^{eff} takes into account a correction term arising from the free-carrier polarization in the field.

The Edwards–Loveluck occupation operators[38] $\xi_i=(0,1)$ describe the magnetic dilution. Namely, $\xi_i=0$ corresponds to the magnetic vacancy in the ith lattice site and $\xi_i=1$ describes the state when the ith lattice site is occupied by the spin S_i^α. These operators are subject to configurational averaging $\langle\ldots\rangle_r$, which we assume to be independent of the magnetic structure. On the other hand, the spin operators S_i^α, for a given atomic configuration, are subject to thermal averaging $\langle\ldots\rangle$ only.

The configurational averaging of single-site occupation operators can be conveniently described by introducing a parameter $n=\langle\xi_i\rangle_r$, where n is the concentration of the magnetic component. The parameter n can be regarded as a ratio of the number of magnetic atoms to the total number of lattice sites. For simplicity, we will further assume that n is equal for both sublattices ($\alpha=a,b$). In turn, the configurational averaging of $(\xi_i\xi_j)$ pairs leads to the following expression:

$$\langle\xi_i\xi_j\rangle_r = n^2 + \Delta_k, \tag{2}$$

where $\xi_i=\langle\xi_i\rangle_r+\delta\xi_i$, and $\Delta_k=\langle\delta\xi_i\delta\xi_j\rangle_r$ is a fluctuation of the occupation numbers, which is characteristic for the kth coordination zone. As has been shown in the Appendix, the fluctuations must obey the sum rule

$$\sum_k z_k\Delta_k = 0, \tag{3}$$

where z_k is the total number of lattice sites on the kth coordination zone where the fluctuation Δ_k takes place. These fluctuations are connected with the Warren–Cowley (WC) short-range-order (SRO) parameter[39] α_k by the following relationship:

$$\alpha_k = \frac{\langle\xi_i\xi_j\rangle_r - \langle\xi_i\rangle_r\langle\xi_j\rangle_r}{\langle\xi_i\rangle_r\langle\xi_j\rangle_r} = \frac{\Delta_k}{n^2}. \tag{4}$$

In the approximation in which $\Delta_k=0$, the distribution of magnetic ions over the lattice is fully stochastic. A detailed analysis of the physical range of WC parameter resulting from the pair probability distribution $p(\xi_i\xi_j)$ is presented in the Appendix.

As far as the thermal averaging of the spin operators is concerned, we will adopt the simplest molecular field approximation (MFA), with the decoupling relation $\langle S_i^\alpha S_j^\beta\rangle \approx m^\alpha m^\beta$, where α (or β)$=a,b$ and $m^\alpha=\langle S_i^\alpha\rangle$ denotes α-sublattice magnetization. The MFA is justified by the presence of long-range interaction (for the infinite interaction range, it becomes an exact method) and by the sublattice model of antiferromagnetism according to the idea of Néel. As far as we know,[32–34] in the fcc structure, apart from the ferromagnetic (F) and paramagnetic (P) phases, nothing impedes the notion that different antiferromagnetic orderings exist. The most known seem to be the antiferromagnetic first kind (AF1), antiferromagnetic first kind improved (AF1I), and antiferromagnetic second kind (AF2) orderings. We put emphasis on the fact that we are only interested in thermodynamically stable phases here, excluding the possible existence of metastable states of the spin-glass kind.

Within MFA, the magnetic enthalpy can be found by the configurational and thermal averaging of the Hamiltonian (1). The result is

$$\begin{aligned} H &= \langle\langle\mathcal{H}\rangle\rangle_r \\ &= -\frac{N}{4}\sum_k J_k z_k^{\uparrow\uparrow}(n^2+\Delta_k)[(m^a)^2+(m^b)^2] \\ &\quad -\frac{N}{2}\sum_k J_k z_k^{\uparrow\downarrow}(n^2+\Delta_k)m^a m^b - \frac{N}{2}n(m^a+m^b)h. \end{aligned} \tag{5}$$

By N we denote the total number of lattice sites, whereas the summation upon k is performed over all coordination zones centered at the arbitrary lattice site. In Eq. (5), $z_k^{\uparrow\uparrow}$ ($z_k^{\uparrow\downarrow}$) are the number of lattice sites on the kth coordination zone, whose spins (if occupied) are oriented parallel (antiparallel) to the central spin. Thus, $z_k^{\uparrow\uparrow}$ is the coordination number at the kth zone formed from lattice sites belonging to the same magnetic sublattice as the central spin, while $z_k^{\uparrow\downarrow}$ is the coordination number formed from lattice sites belonging to different sublattices. Those numbers satisfy the condition $z_k^{\uparrow\uparrow}+z_k^{\uparrow\downarrow}=z_k$ and their distribution upon k depends on the type of magnetic ordering (F, AF1, AF1I, or AF2). The numbers can be easily found by a computer program analyzing the structure.

The exchange integral J_k in Eq. (5) for a given coordination zone k is basically the RKKY long-range interaction, with the exception of the first coordination zone, where we additionally include the antiferromagnetic (AF) superexchange interaction $J^{\text{AF}}<0$. This kind of interaction has been introduced in several papers[10–14,16] concerning DMSs. Thus, we assume that $J_1=J^{\text{AF}}+J_1^{\text{RKKY}}$ for $k=1$ and $J_k=J_k^{\text{RKKY}}$ for $k=2,3,\ldots$, where the RKKY interaction is given by the expression[40]

$$J_k^{\text{RKKY}} = C(k_F a)^4 \frac{\sin(2k_F r_k) - 2k_F r_k\cos(2k_F r_k)}{(2k_F r_k)^4} e^{-r_k/\lambda}. \tag{6}$$

In Eq. (6), a is the lattice constant and r_k stands for the radius of the kth coordination zone. The Fermi wave vector k_F for the fcc structure takes the form $k_F=(12\pi^2 n)^{1/3}/a$, where we assume that each occupied lattice site yields one charge carrier to the conduction or valence band. Thus, we assume that the free carrier concentration is n, i.e., the same as the concentration of magnetic atoms in the fcc lattice. The energy constant $C=A^2m^*/2\pi^3\hbar^2a^4$ in Eq. (6) can be treated as the unit energy, for the exchange integral and for the k_BT scale as well. As far as the exponential factor in Eq. (6), containing the damping parameter λ, is concerned, such a term has been introduced by Mattis[9] in order to account for the charge carrier localization in disordered systems. It follows from the

literature[7,41] that such a localization takes place in some DMSs, such as $Ga_{1-x}Mn_xAs$. The above description of J_k for $k=1,2,\ldots$, defines the so-called modified RKKY interaction, the model which has successfully been used in several papers concerning DMS systems.[11–14,16]

The magnetic enthalpy (5) allows the study of the ground-state phase diagrams (for $T\to 0$) when a perfect spin alignment is assumed (for instance, $m^a=S$ and $m^b=-S$ for the antiferromagnetic phase). By comparing the enthalpy values for different magnetic phases (F, P, AF1, AF1I, and AF2), the stability areas for each phase can be established from the minimum condition. The magnetic phase diagram can be obtained vs concentration n, fluctuation distribution Δ_k, and external field h for the given parameters J^{AF} and λ characterizing the modified RKKY interaction. For instance, for the antiferromagnetic phases in the ground state, the enthalpy per lattice site is given by the following expression:

$$\frac{H}{N}=-\frac{1}{2}n^2S^2\sum_k(1+\alpha_k)(z_k^{\uparrow\uparrow}-z_k^{\uparrow\downarrow})J_k, \tag{7}$$

where α_k is the WC parameter for the kth coordination zone and $z_k^{\uparrow\uparrow}$ ($z_k^{\uparrow\downarrow}$) depend on the type of the antiferromagnetic phase. On the other hand, for the ferromagnetic phase in the ground state (when $m^a=m^b=S$), the corresponding formula for the enthalpy reads

$$\frac{H}{N}=-\frac{1}{2}n^2S^2\sum_k(1+\alpha_k)z_kJ_k-g^{\mathrm{eff}}\mu_BH^zSn. \tag{8}$$

The sign of the Zeeman-like term in Eq. (8) selects the energetically favorable orientation of spins toward the external field $H^z>0$. Obviously, due to the antiferromagnetic symmetry, this term vanishes in Eq. (7). In turn, for the paramagnetic phase (with $m^\alpha=0$), we assume $H/N=0$.

The long-range interaction requires the numerical summation over all coordination zones $k=1,2,\ldots,k_{\max}$, where $k_{\max}$ corresponds to some cutoff radius $r_{\max}$ for which the energy per lattice site is satisfactorily convergent. The numerical convergency of the exchange energy within a sufficiently large radius $r_{\max}$ for which the indirect interactions practically vanish makes the calculations in the ground state nearly exact. The numerical calculations of the ground-state phase diagrams with the structural ordering taken into account will be presented in the next section.

As far as the temperature studies are concerned, one has to consider not only the temperature dependencies of the sublattice magnetizations m^α ($\alpha=a,b$) but also the magnetic entropy. In the MFA method, a unified approach can be suggested, based on the single-site density matrix

$$\rho_i^\alpha=\frac{\exp[\beta(\Lambda^\alpha+h)S_i^\alpha]}{Z_1^\alpha}, \tag{9}$$

where $\beta=1/k_BT$, and Λ^α is a variational parameter of the molecular field acting on the α sublattice. The single-site partition function Z_1^α for the α sublattice is defined by the following formula:

$$Z_1^\alpha=\mathrm{Tr}_i\{\exp[\beta(\Lambda^\alpha+h)S_i^\alpha]\}=\sum_{l=-S}^{S}\exp[\beta(\Lambda^\alpha+h)l]. \tag{10}$$

Then, the total partition function Z in the MFA is given by the product $Z=(Z_1^aZ_1^b)^{Nn/2}$, where $Nn/2$ is the number of lattice sites occupied within one sublattice. With the use of the single-site density matrix (9), the various thermal mean values can be calculated. For instance, the magnetization of the occupied site on the α sublattice is

$$m^\alpha=\mathrm{Tr}_i[S_i^\alpha\rho_i^\alpha]=\frac{1}{Z_1^\alpha}\mathrm{Tr}_i\{S_i^\alpha\exp[\beta(\Lambda^\alpha+h)S_i^\alpha]\}, \tag{11}$$

which leads to the general formula

$$m^\alpha=SB(S\beta(\Lambda^\alpha+h)), \tag{12}$$

where $\alpha=a,b$ and $SB(x)$ is the Brillouin function for an arbitrary spin S as follows:

$$SB(Sx)=\frac{2S+1}{2}\coth\left(\frac{2S+1}{2}x\right)-\frac{1}{2}\coth\left(\frac{x}{2}\right). \tag{13}$$

Due to the factorization in MFA, the total entropy σ can be presented as a sum of single-site entropies for both sublattices as follows:

$$\sigma=\frac{N}{2}n\sum_{\alpha=a,b}\sigma_1^\alpha. \tag{14}$$

The single-site entropy σ_1^α for the occupied site on the α sublattice is given by the thermal mean value

$$\sigma_1^\alpha=-k_B\langle\ln\rho_i^\alpha\rangle=-k_B\,\mathrm{Tr}_i(\rho_i^\alpha\ln\rho_i^\alpha). \tag{15}$$

Making use of Eq. (9), the single-site entropy σ_1^α can be presented in the following form:

$$\sigma_1^\alpha=-\frac{1}{T}(\Lambda^\alpha+h)m^\alpha+k_B\ln Z_1^\alpha. \tag{16}$$

Hence, the total entropy (14) can be presented as follows:

$$\sigma=\frac{N}{2}n\frac{1}{T}[-(\Lambda^a+h)m^a-(\Lambda^b+h)m^b+k_BT\ln Z_1^a+k_BT\ln Z_1^b]. \tag{17}$$

Having calculated the entropy (17) and the enthalpy (5), the Gibbs free energy can be found in MFA from the following thermodynamic formula:

$$G=H-\sigma T. \tag{18}$$

However, with a view to constructing the phase diagrams, we are interested in the Gibbs energy per lattice site, i.e., in the chemical potential μ, which is then given by

$$\mu = \frac{G}{N}$$
$$= -\frac{1}{4}n^2\sum_k J_k z_k^{\uparrow\uparrow}(1+\alpha_k)[(m^a)^2+(m^b)^2]$$
$$-\frac{1}{2}n^2\sum_k J_k z_k^{\uparrow\downarrow}(1+\alpha_k)m^a m^b + \frac{n}{2}(\Lambda^a m^a + \Lambda^b m^b)$$
$$-\frac{n}{2}k_B T(\ln Z_1^a + \ln Z_1^b). \quad (19)$$

The molecular field (variational) parameters Λ^α appearing in Eqs. (19), (12), and (10) can be determined from the necessary extremum conditions:

$$\frac{\partial\mu}{\partial\Lambda^\alpha} = 0 \quad (20)$$

(for $\alpha=a,b$), which lead to the following expressions:

$$\Lambda^a = \sum_k J_k(1+\alpha_k)(z_k^{\uparrow\uparrow}m^a + z_k^{\uparrow\downarrow}m^b) \quad (21)$$

and

$$\Lambda^b = \sum_k J_k(1+\alpha_k)(z_k^{\uparrow\uparrow}m^b + z_k^{\uparrow\downarrow}m^a). \quad (22)$$

Now, with the help of Eqs. (21) and (22), the chemical potential (19) for the thermodynamical equilibrium is obtained in the final form as follows:

$$\mu = \frac{1}{4}n^2\sum_k J_k z_k^{\uparrow\uparrow}(1+\alpha_k)[(m^a)^2+(m^b)^2]$$
$$+\frac{1}{2}n^2\sum_k J_k z_k^{\uparrow\downarrow}(1+\alpha_k)m^a m^b - \frac{n}{2}k_B T(\ln Z_1^a + \ln Z_1^b) \quad (23)$$

together with Z_1^α given by Eq. (10) and m^α as a solution of Eq. (12).

From this point on, the expression (23) for the chemical potential allows the self-consistent studies of all the thermodynamic properties in MFA. Let us note first that the necessary equilibrium conditions for the chemical potential (20) are also satisfied with respect to the sublattice magnetization: $\partial\mu/\partial m^\alpha = 0$ ($\alpha=a,b$). Moreover, the mean magnetization per lattice site m can be derived as an alternative to Eqs. (11) and (12) merely by differentiating the chemical potential over the external field as follows:

$$m = \left(\frac{\partial\mu}{\partial h}\right)_T = \frac{1}{2}n(m^a + m^b). \quad (24)$$

Analogously, by differentiating the chemical potential over the temperature the mean entropy per lattice site can be calculated, yielding the same form as Eqs. (14) and (17), as follows:

$$\frac{\sigma}{N} = \left(\frac{\partial\mu}{\partial T}\right)_h = \frac{1}{2}n(\sigma_1^a + \sigma_1^b). \quad (25)$$

Consequently, other thermodynamic properties such as the magnetic susceptibility or magnetic contribution to the specific heat can be calculated as the second-order derivatives of the chemical potential (23).

The critical temperature of the second-order (continuous) phase transitions can be obtained from the linearization of Eq. (12) for $h=0$ and $m^\alpha \to 0$. Making use of the linear expansion for the Brillouin function $SB(Sx) \overset{(x\to 0)}{\to} S(S+1)x/3$, we obtain from Eq. (12) the following:

$$m^\alpha = \frac{S(S+1)}{3}\beta_c\Lambda^\alpha \quad (26)$$

($\alpha=a,b$), where $\beta_c = 1/k_B T_c$ and T_c is the critical temperature. Now, by substituting Λ^α from Eqs. (21) and (22) into Eq. (26), we obtain a set of two linear, homogeneous equations for $m^\alpha \to 0$ in the vicinity of T_c. Next, by setting the determinant equal to zero, the phase transition temperature T_c is derived in the following form:

$$k_B T_c = \frac{S(S+1)}{3}n\sum_k J_k(1+\alpha_k)(z_k^{\uparrow\uparrow} \pm z_k^{\uparrow\downarrow}). \quad (27)$$

Equation (27) is a generalization of the MFA result for the long-range RKKY interaction with the structural clustering taken into account. The solution with "+" corresponds to the Curie temperature and is applicable to a ferromagnetic phase transition, whereas the solution with "−" corresponds to the Néel temperature for the antiferromagnetic (AF1, AF1I, and AF2) phase boundaries. The temperature phase diagrams based on Eq. (27) will be calculated in the next section.

III. NUMERICAL RESULTS AND DISCUSSION

The extensive numerical studies have been carried out for the model fcc structure, with dilution and the modified RKKY interaction taken into account. We recall the assumption that each magnetic impurity atom delivers one free carrier mediating the interaction.

A. Ground-state phase diagrams for $h=0$

The ground-state phase diagrams have been calculated on the basis of the exact expressions [Eqs. (7) and (8)] for the external field $h=0$, where the summation over k has been carried out for the long-range interaction extending up to $r_{\max}=150a$. For such an interaction range (which corresponds to 41 253 coordination spheres in the fcc structure), we assure the perfect numerical convergence of the enthalpy per lattice site with special regard to the low concentration range. Thus, the numerical results are nearly exact.

According to the theoretical considerations, when the dilution is not random, it cannot be described by only a single variable n, but should be characterized by the set of Warren–Cowley SRO parameters. These parameters, α_k, which are incorporated into the analytical formulas in the previous section, fulfill the sum rule [Eq. (3)] and are treated as indepen-

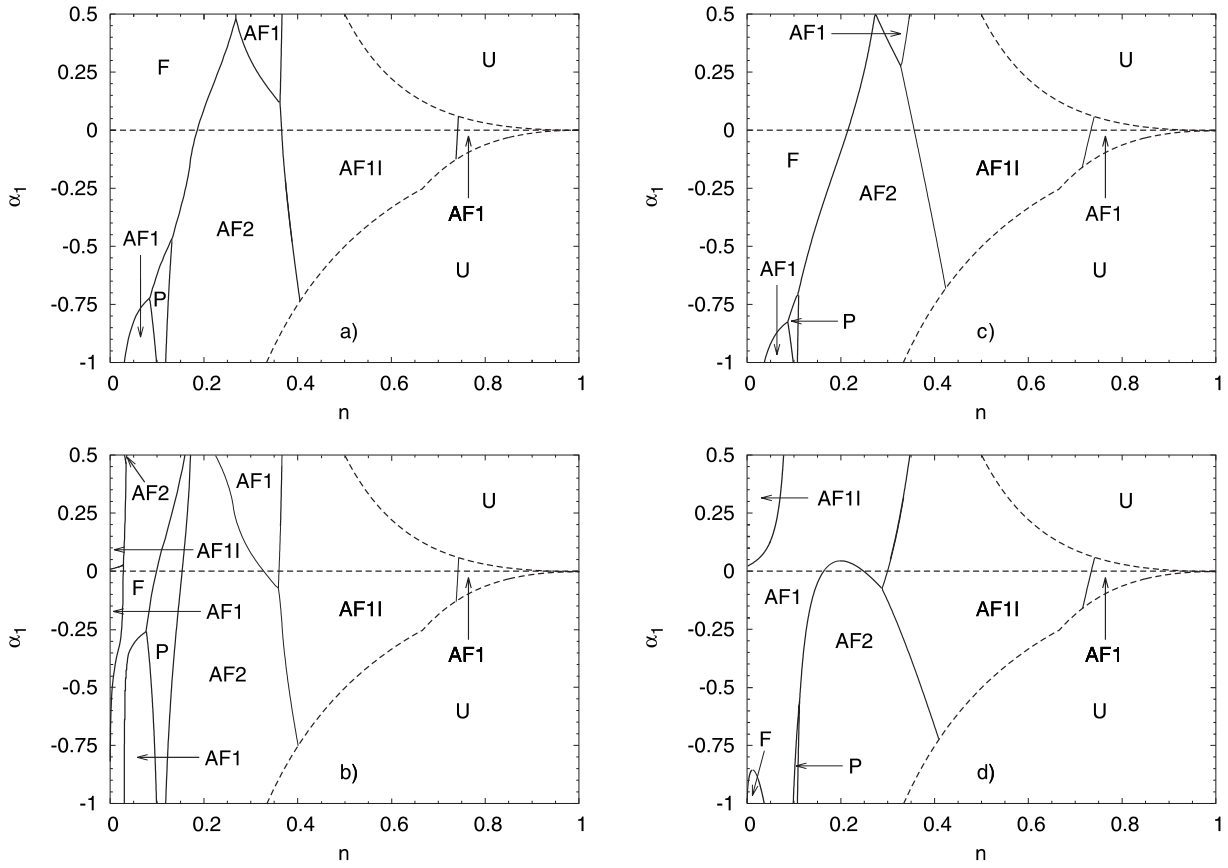

FIG. 1. Ground-state magnetic phase diagrams in the (n,α_1) plane for different values of parameters modifying the RKKY interaction: (a) $\lambda\to\infty$, $J^{\mathrm{AF}}=0$; (b) $\lambda\to\infty$, $J^{\mathrm{AF}}/C=-0.5$; (c) $\lambda/a=1.0$, $J^{\mathrm{AF}}=0$; and (d) $\lambda/a=1.0$, $J^{\mathrm{AF}}/C=-0.5$. By U we denote an unphysical area for the α_1 parameter.

dent of the magnetic structure. However, for the simplicity of numerical calculations, we will further assume that only α_1 and α_2 parameters are different from zero, while $\alpha_k=0$ for $k>2$. Such assumption reflects the empirical fact that the structural correlations for two first coordination zones are the most important factors. In this way, only α_1 becomes an independent SRO parameter of the theory [with some constraints imposed, as discussed in the Appendix; see Eq. (A16) and Fig. 9], whereas α_2 is determined from the sum rule $\alpha_2=-(z_1/z_2)\alpha_1$.

The stability regions for the phases (F, P, AF1, AF1I, and AF2), where the enthalpy of each phase is minimal, have been found in the (n,α_1) plane, and the results are presented in Fig. 1. Figures 1(a)–1(d) correspond to the different parameters of the modified RKKY interaction, as indicated in the figure caption. In the figure, the unphysical (U) area of the Warren–Cowley parameter α_1 vs charge carrier concentration n is depicted and delimitated by the dashed lines. The origin of that area is discussed in the Appendix. The horizontal dashed line for $\alpha_1=0$ corresponds to the absence of SRO. The occurrence of phases and their sequence for $\alpha_1=0$ upon n is in agreement with those studied in Refs. 35 and 37, where the SRO was not taken into account.

Figure 1(a) is prepared for $\lambda\to\infty$ and $J^{\mathrm{AF}}=0$, i.e., for the "pure" RKKY interaction. The F phase is present for the low concentration n only, but for all values of α_1. The positive α_1 values (with structural clustering) enlarges the stability of the F phase. On the other hand, for $\alpha_1<0$, the antiferromagnetic phases become more favorable and even the P phase can occur in some small restricted area. There are three stability regions for the AF1 phase in Fig. 1(a). The rest of the phases occur in the single regions only. In Fig. 1(b), the antiferromagnetic NN interaction, with the value $J^{\mathrm{AF}}/C=-0.5$, is included. As a result, the F-phase area is strongly reduced, whereas the antiferromagnetic phases are extended. There are four stability regions for the AF1 phase and two for each AF1I and AF2. The new areas (AF1, AF1I, and AF2) appear for the lowest values of n. Moreover, the P phase becomes stable over all values of α_1 in some narrow range of concentrations n. In Fig. 1(c), we assume $J^{\mathrm{AF}}=0$ and $\lambda/a=1$, which represent a relatively strong charge carrier localization. The topology of this diagram is somewhat similar to Fig. 1(a), with some differences in the shapes of the particular lines. Two areas of antiferromagnetic AF1 phases (one for strong negative and the other for strong positive α_1 parameters) are smaller than the corresponding areas in Fig. 1(a), i.e., without the RKKY damping. In Fig. 1(d), both nonzero values of $J^{\mathrm{AF}}/C=-0.5$ and $\lambda/a=1$ were assumed. As a result, the F and P phases have been reduced to the smallest areas. It is seen that for the positive structural clustering, with $\alpha_1>0$, only the antiferromagnetic phases are favored in Fig. 1(d). There are two AF1 and also two AF1I areas which are stable for these phases in Fig. 1(d). The AF1 region has remarkably

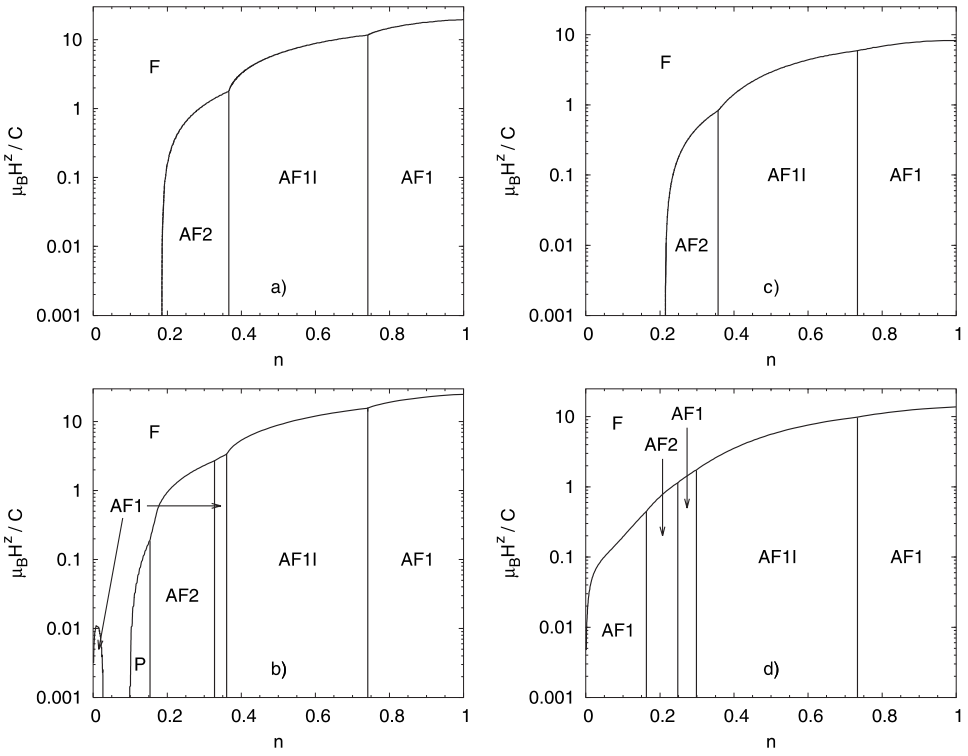

FIG. 2. The phase diagram vs external field and impurity concentration, for $\alpha_1=0$ and different values of parameters modifying the RKKY interaction: (a) $\lambda\to\infty$, $J^{AF}=0$; (b) $\lambda\to\infty$, $J^{AF}/C=-0.5$; (c) $\lambda/a=1.0$, $J^{AF}=0$; and (d) $\lambda/a=1.0$, $J^{AF}/C=-0.5$.

increased, whereas the AF2 phase has been limited, mainly to the negative SRO parameters.

From the analysis of Figs. 1(a)–1(d), some general conclusions can be drawn. The SRO parameter exerts a strong influence on the phase diagram, but not for all values of n on equal footing. The greatest changes are observed for small n values, i.e., for strong dilution. Both J^{AF} and λ parameters, which modify the RKKY interaction, also have an important meaning, which is manifested in Fig. 1 by remarkable divergences between various parts [(a)–(d)] of the figure. All the phase boundaries presented in Fig. 1 constitute the discontinuous (first order) phase transitions.

B. Ground-state phase diagrams in the external field

Next we studied the influence of the external field on the phase boundaries. We present here a specific case of spatially uncorrelated impurities, where Eqs. (7) and (8) have been employed for $\alpha_k=0$. Here, it was sufficient to perform the summation up to $r_{max}=100a$ (i.e., 18 335 coordination spheres in the fcc structure). For the Zeeman term, some values of the material constants had to be accepted to enable numerical calculations. As an example, we assumed the experimental values characteristic for $Ga_{1-x}Mn_xAs$.[6,42,43] They are $a=5.65$ Å, $A=-55$ meV nm^3, $m^*=0.5m_e$, and $S=5/2$. For such values, the energetic constant in Eq. (6) amounts to $C=3.1$ meV, while the magnetic field constant $C/\mu_0\mu_B=540$ kOe. The numerical results presenting the stability areas for various phases in the ground state are presented in Figs. 2–4.

The first diagram [Fig. 2(a)] corresponds to the pure RKKY interaction, i.e., without any damping ($\lambda=\infty$) and without the NN superexchange coupling ($J^{AF}=0$). The influence of the external field (in dimensionless units and logarithmic scale) on the stability of various phases, which occur for different magnetic impurity concentrations, is shown. For $H^z=0$, we obtain the phase sequence and the position of the phase boundaries exactly the same as discussed in the paper.[35] It can be seen from Fig. 2 that in the sufficiently strong field, the F phase becomes dominant. For $H^z=0$, this F phase originates from the low n concentration region.

In Fig. 2(b), the NN superexchange antiferromagnetic interaction is taken into account with some moderate value ($J^{AF}/C=-0.5$). The RKKY damping is again neglected ($\lambda=\infty$). Comparing Figs. 2(b) and 2(a), we notice an important influence of the J^{AF} parameter on the diagram. First of all, the F phase in the small field is confined between the AF1 and P phases. The existence of a P phase in the ground state is noteworthy, indicating that a spin-glass state might be possible for low temperatures. The AF1 phase in Fig. 2(b) occupies three new areas, instead of one area, as in Fig. 2(a).

In Fig. 2(c), a relatively strong damping of the RKKY interaction is incorporated with the value $\lambda/a=1$. Comparing Figs. 2(a) and 2(c), we observe that, as a result of damping, the F phase slightly enlarges its area at the expense of the antiferromagnetic phases. The phase boundaries between the antiferromagnetic phases are represented by the straight vertical lines, which reflects their independence of the field [see Eq. (8)].

By including a strong damping ($\lambda/a=1$) together with $J^{AF}/C=-0.5$ in Fig. 2(d), the phase diagram changes drastically in comparison with Fig. 2(b). The P phase disappears and an AF1 phase spreads up; as a result, the F phase for $H^z=0$ is completely eliminated. Also, the area of the AF2 phase becomes much smaller. However, for a sufficiently strong field, the F phase is recovered, as in the previous

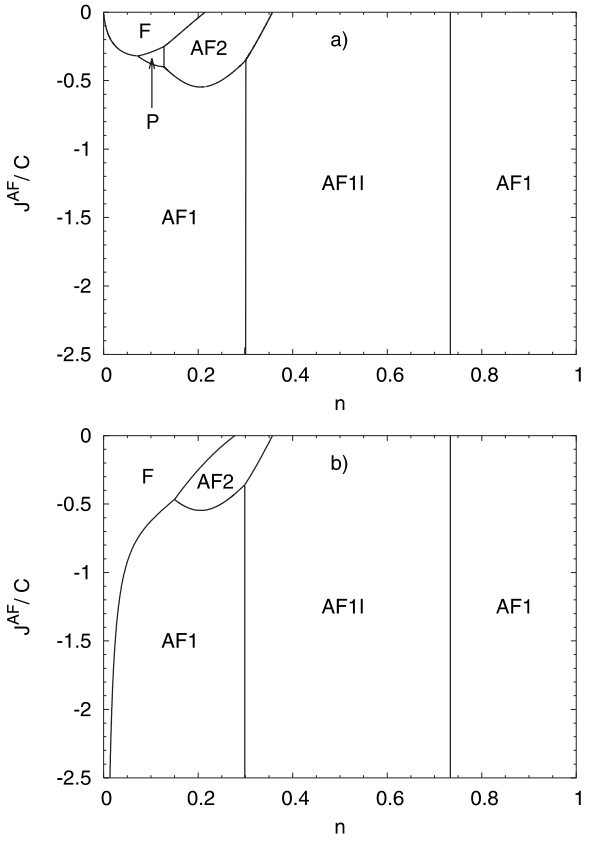

FIG. 3. The phase diagram vs NN antiferromagnetic interaction energy and impurity concentration, for $\lambda/a=1.0$ and (a) $H^z=0$ and (b) $\mu_B H^z/C=0.3$.

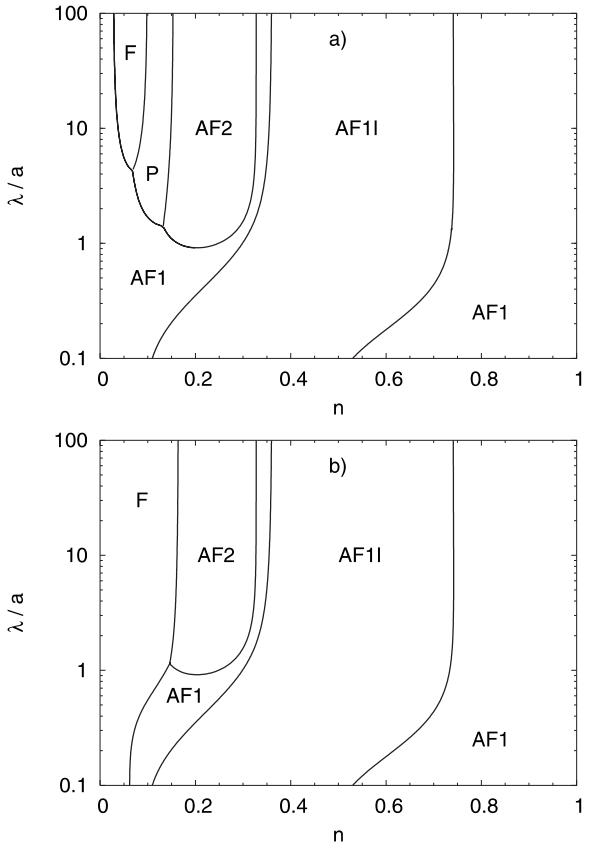

FIG. 4. The phase diagram vs damping length scale and impurity concentration, for $J^{AF}/C=-0.5$ and (a) $H^z=0$ and (b) $\mu_B H^z/C=0.3$.

figures. By comparing Fig. 2(a)–2(d), one can also conclude that the damping exerts a much greater effect on the diagram for $J^{AF}/C=-0.5$ than for $J^{AF}=0$. On the other hand, Figs. 2(c) and 2(d) (with the same damping parameter $\lambda/a=1$) show that, in this case, the influence of J^{AF} becomes quite remarkable. It is worth noticing that all these relevant changes presented in Figs. 2(a)–2(d) concern mainly the low n concentration region (which is the range of practical interest in DMS).

The effect of switching the external field on and off is demonstrated in Figs. 3 and 4. In Fig. 3, the phase diagram in $(n, J^{AF}/C)$ coordinates is presented, whereas $\lambda/a=1$ for (a) $H^z=0$ and for (b) $\mu_B H^z/C=0.3$. In particular, in Fig. 3(a), the influence of the negative superexchange NN interaction, J^{AF}, on the phase diagram is shown. For a sufficiently large value of this interaction, the phases F, P, and AF2 vanish, and only two phases (AF1 and AF1I) remain. By switching a relatively strong field on in Fig. 3(b), we are able to maintain the F and AF2 phases; however, the P phase is not present. We see in Fig. 3(b) that the F phase extends over a larger area than in Fig. 3(a), which results from the interaction of this phase with the field.

In Fig. 4, the phase diagram in $(n, \lambda/a)$ coordinates is presented, whereas $J^{AF}/C=-0.5$ for (a) $H^z=0$ and for (b) $\mu_B H^z/C=0.3$. In this case, the influence of damping factor λ is demonstrated for various concentrations n of impurity spins. For $H^z=0$ [in Fig. 4(a)], a variety of phases is shown and even the P phase is present. Without the external field and for a relatively strong damping, the three phases (F, P, and AF2) vanish. For low carrier concentrations, it could be worth mentioning that the behavior of the ferromagnetic phase, which can be destroyed by increasing the carrier localization degree (i.e., decreasing λ), resembles some experimental findings in $Ga_{1-x}Mn_xAs$, where the onset of the ferromagnetic phase is related to the transition from insulating to metallic state.[6] When the field is switched on [in Fig. 4(b)], the F phase extends over a small concentration region for all λ values and the P phase disappears. However, the AF2 phase remains, admittedly, in a slightly smaller area than in Fig. 4(a). Again, the most interesting changes presented in Figs. 3 and 4 concern the region of small concentrations n.

C. Critical temperature

The transition temperature from a spontaneously ordered to a disordered state is calculated on the basis of Eq. (27). In connection with the ground-state phase diagrams, the most important changes are predicted for small n values; therefore, we will present the results of critical temperature calculations in the range of $n \leqslant 0.25$. In Figs. 5(a)–5(d), the reduced critical temperature $T_c/[nS(S+1)C]$ vs n is presented for the same parameters of modified RKKY interaction as in Figs.

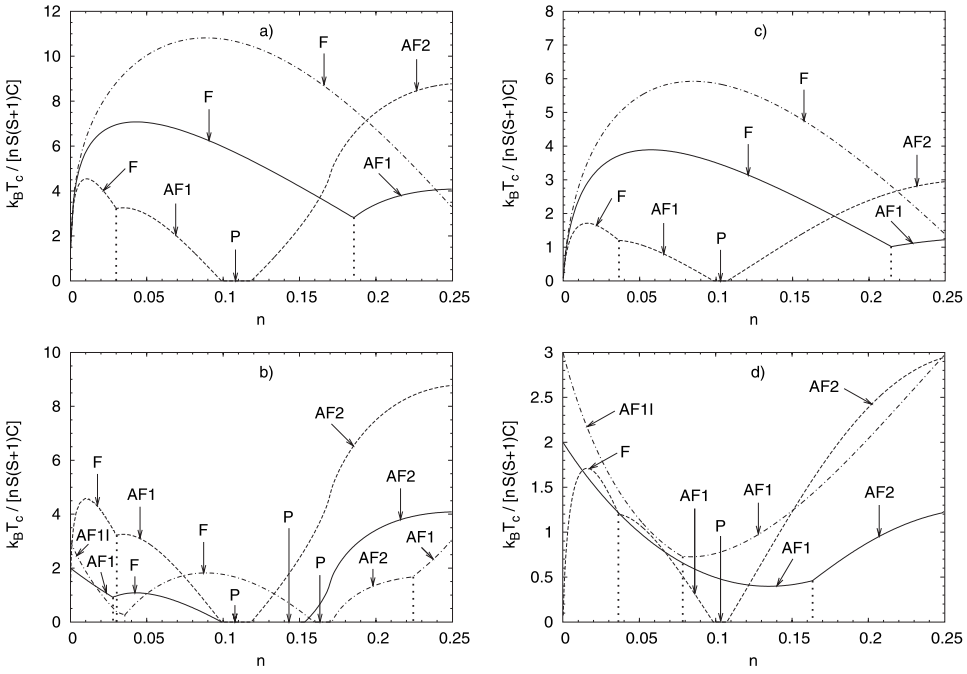

FIG. 5. MFA reduced critical temperature vs charge carrier concentration, for different values of parameters modifying the RKKY interaction: (a) $\lambda \to \infty$, $J^{AF}=0$; (b) $\lambda \to \infty$, $J^{AF}/C=-0.5$; (c) $\lambda/a=1.0$, $J^{AF}=0$; and (d) $\lambda/a=1.0$, $J^{AF}/C=-0.5$ and for different structural correlations: $\alpha_1=0$ (solid line), $\alpha_1=-1.0$ (dashed line), and $\alpha_1=0.5$ (dashed-dotted line).

1(a)–1(d), respectively. The reduced temperature provides the results independent of the spin magnitude S and shows a nonlinear dependency of T_c on n. On each phase diagram [Figs. 5(a)–5(d)], the three curves are presented: solid, dashed, and dashed-dotted lines for $\alpha_1=0$, -1 and 0.5, respectively. Thus, the temperature phase diagrams in Fig. 5 are prepared as the horizontal cross sections for the corresponding ground-state phase diagrams presented in Fig. 1. The values of α_1 have been chosen on the basis that they enable one to compare the calculations for the extremal SRO parameters ($\alpha_1=-1$ and $\alpha_1=0.5$) with that for the absence of SRO ($\alpha_1=0$). The critical temperatures for each specific phase in Fig. 5 are pointed by the arrows with the phase symbols. The vertical (dotted) lines indicate the discontinuous phase boundaries, from P phase down to the ground state, and their positions on n are in agreement with Fig. 1.

Some interesting features observable in Fig. 5 should be emphasized. In particular, in Fig. 5(a), for the unmodified RKKY interaction, it is seen that the positive clustering increases the Curie temperature and makes the region of the F phase wider. On the other hand, the negative structural correlations reduce the Curie temperatures and the width of the ferromagnetic region. For the negative SRO parameters, with the increase of n, a relatively high Néel temperature for the AF2 phase can be achieved.

For the antiferromagnetic NN interaction with the value $J^{AF}/C=-0.5$ [Fig. 5(b)], the situation seems somewhat more complicated. The ferromagnetic phase for $\alpha_1=0$ and $\alpha_1=0.5$ is weaker than for the corresponding cases in Fig. 5(a); however, for $\alpha_1=-1$, it has a very similar phase boundary. The characteristic features are three paramagnetic gaps (one for each curve) occurring in accordance with Fig. 1(b). Also, for the small values of n, the new phases AF1 and AF1I are perceptible, with their Néel temperatures decreasing with the increase of magnetic impurity (and charge) concentration n. In Fig. 5(c), the influence of the charge carrier localization (with $\lambda/a=1$) on the Curie temperature is demonstrated. When compared with Fig. 5(a), a remarkable reduction of all critical temperatures is apparent although the influence of SRO on the ground-state phase boundary shapes is comparable [see Figs. 1(a) and 1(c)] over the presented range of n. In Fig. 5(d), when both nonzero parameters ($J^{AF}/C=-0.5$ and $\lambda/a=1$) are taken into account, the ferromagnetic phase is present only for $\alpha_1=-1$. For all curves in Fig. 5(d), a minimum of T_c is present in the region of concentrations for $n \approx 0.07-0.15$.

All the phase transitions from ordered state to paramagnetic state, shown in Fig. 5, are continuous (second order) ones. However, for the vertical (dotted) lines, the perpendicular phase transitions (for constant temperature) between different ordered states are of discontinuous character, starting from the P phase down to the ground state. The points of junction, where two different second-order phase transition lines merge with another first-order phase transition line, are usually called the bicritical points. It can be noted that with the change of concentration n, the phase transition temperatures can either increase or decrease and the changes are strongly nonlinear. This effect depends not only on the range of concentration n but on the SRO parameter as well.

D. Magnetic frustration

Magnetic frustration is unavoidable for systems with the long-range oscillatory interaction. The presence of frustration leads to the increase of magnetic energy and decrease of the critical temperature. In order to define quantitatively the degree of frustration, we introduce an "ideal" ground-state energy E_0 in the following form:

$$E_0 = -n^2S^2\sum_{\langle i,j\rangle}|J(r_{ij})| = -n^2S^2\frac{N}{2}\sum_k z_k|J_k|. \qquad (28)$$

E_0 is the lowest magnetic energy which would be achieved in the hypothetical case, when no frustrations were present in

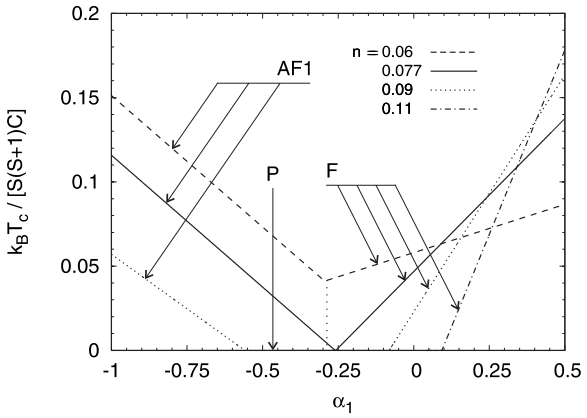

FIG. 6. MFA critical temperature in the vicinity of a selected triple point, $(n,\alpha_1)=(0.077,-0.25)$ from Fig. 1(b), vs the Warren–Cowley parameter α_1 for various charge carrier concentrations n.

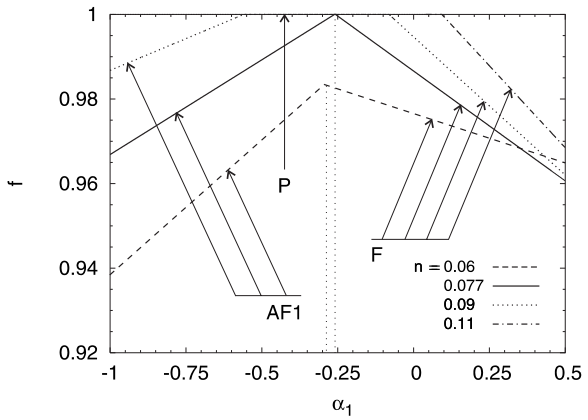

FIG. 7. Degree of frustration f in the vicinity of a selected triple point, with the same parameters as in Fig. 6, vs the Warren–Cowley parameter α_1 for various charge carrier concentrations n.

the system. However, the real internal energy in the frustrated ground state, $E_g=(H)_{h=0}$, is given by the formulas (7) and (8) for the external field $h=0$. Thus, we can define the degree of frustration f in the ground state as follows:

$$f=\left|\frac{E_g-E_0}{E_0}\right|. \tag{29}$$

The value of f comes from the range $\langle 0;1\rangle$, where $f=0$ is for the ideal unfrustrated system, and $f=1$ stands for the paramagnetic phase with $E_g=0$.

In order to demonstrate a correlation of the degree of frustration with the phase transition temperature, first, in Fig. 6, we present the four reduced T_c curves for different n parameters, where $J^{\mathrm{AF}}/C=-0.5$ and $\lambda\to\infty$. The choice of n parameters ($n=0.06$, 0.077, 0.09, and 0.11) enables the vertical scan of Fig. 1(b) upon α_1, in the vicinity of the triple point which has the coordinates $(n,\alpha_1)=(0.077,-0.25)$. In this triple point in Fig. 1(b), the three phases: F, AF1, and P do coexist. The temperature studies in Fig. 6 show both Néel and Curie temperatures, as well as the existence of paramagnetic (P) phase, where $T_c=0$. On the other hand, in Fig. 7, the degree of magnetic frustration f in the ground state is presented for the same set of parameters $(J^{\mathrm{AF}},\lambda,n)$ and abscissa axis α_1 as in Fig. 6. By comparison of Figs. 6 and 7, it is seen that the increase (decrease) of the critical temperature is accompanied by the decrease (increase) of the degree of frustration in the ground state, respectively. Both T_c and f are the linear functions of α_1, showing a nonsmooth behavior upon α_1 at the first-order phase transitions. A relatively high degree of frustration in Fig. 7 is remarkable, with its maximum in the vicinity of the triple point. It is worth noticing that at the triple point, the chemical potentials of all coexisting phases are equal and, because of the presence of the P phase, $f=1$.

In order to see how magnetic frustrations are distributed over the (n,α_1) plane, in Fig. 8 the f parameter is presented in the form of iso-f contour lines. The interaction parameters in Fig. 8 amount to (a) ($J^{\mathrm{AF}}=0$, $\lambda\to\infty$), (b) ($J^{\mathrm{AF}}/C=-0.5$, $\lambda\to\infty$), (c) ($J^{\mathrm{AF}}=0$, $\lambda/a=1$), and (d) ($J^{\mathrm{AF}}/C=-0.5$, $\lambda/a=1$), i.e., are the same as in Figs. 1(a)–1(d), respectively. The unphysical range of the SRO parameter is again denoted by U. The iso-f contour lines connect the points with the same value of the frustration parameter f according to the figure legend. In Figs. 8(a) and 8(b), a relatively high value of f can be noticed. On the other hand, in Fig. 8(c), a remarkable reduction of the f parameter can be observed, when compared with Fig. 8(a). It is worthy to remind that respective phase diagrams [Figs. 1(a) and 1(c)] have a similar topology and have been prepared with the difference in λ parameter only. Thus, it is hard to escape the obvious conclusion that the damping of the RKKY interaction reduces the degree of frustration. In contrast, the presence of NN antiferromagnetic interaction on the fcc lattice increases the frustrations, which are then unavoidable even for the neighboring spins. Small white areas in Figs. 8(a)–8(d) with $f=1$ correspond to the paramagnetic phases as also seen in Figs. 1(a)–1(d), respectively. However, the remaining contour lines of f do not reflect the shapes of the ground-state phase boundaries. The distribution of f parameter vs α_1 shows that the SRO has a strong influence on the frustration. However, this effect depends simultaneously on the magnetic dilution n.

The issue of frustration is closely related to the studies of the ground state of DMS. For instance, it provides an explanation for the experimental finding that even at low temperatures the saturation magnetization is significantly lower than the value predicted with the knowledge of the Mn content.[44] This may reflect the noncollinear spin order in $Ga_{1-x}Mn_xAs$ stemming from the frustration in the Heisenberg model.[45]

Regarding the nonferromagnetic orderings, various situations have been reported in the literature for DMS. Different phases of this kind were suggested by Das Sarma *et al.*,[11] either in the regime of a rather high concentration of carriers (which causes the RKKY coupling to exhibit its oscillatory nature even on relatively small distances) or for a large concentration of impurities (when the superexchange short-range interactions dominate) as well as for strong exponential damping. Some of the orderings may possess the features of a spin glass. The problem was also investigated by means of MC simulations for both RKKY and short-range exchange models by Zhou *et al.*[46] We put emphasis on the fact that the

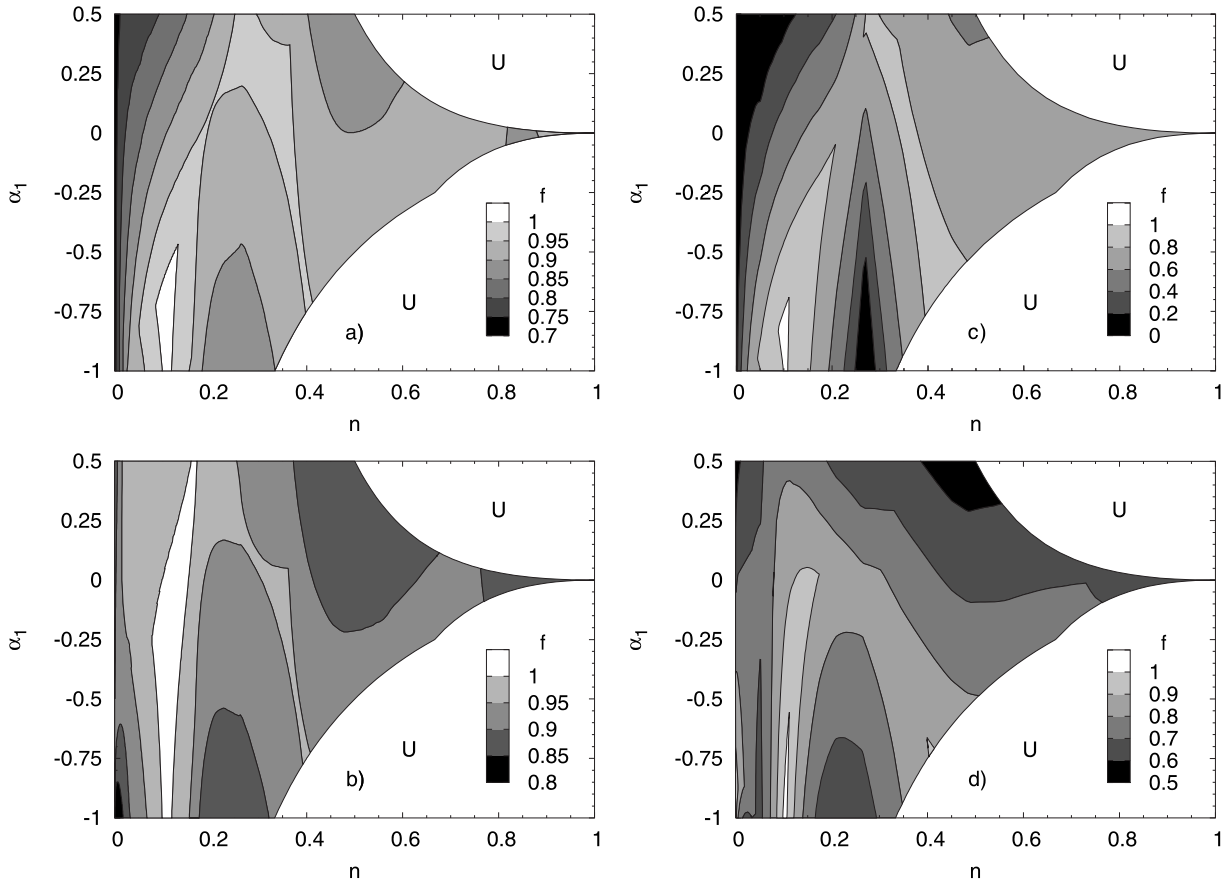

FIG. 8. Distribution of f parameter over (n,α_1) plane for (a) $\lambda\to\infty$, $J^{\mathrm{AF}}=0$; (b) $\lambda\to\infty$, $J^{\mathrm{AF}}/C=-0.5$; (c) $\lambda/a=1.0$, $J^{\mathrm{AF}}=0$; and (d) $\lambda/a=1.0$, $J^{\mathrm{AF}}/C=-0.5$. The contour lines connect points with the same value f of magnetic frustration. Note the differences in f scale in the diagrams.

antiferromagnetic phases existing in our model can appear somewhat similar to a state with randomly oriented spins. Namely, in a site-diluted system with strong dilution, the Ising spins in the antiferromagnetic phase acquire orientations which can be regarded as random due to the probabilistic nature of the occupation of the lattice sites. In our opinion, such diluted phases would be difficult to distinguish from the metastable spin-glass phase being the outcome of MC methods.

E. Other remarks

We strongly emphasize that the actual physical picture of magnetic phenomena in DMS is much more complicated than our model. In these materials, the RKKY mechanism additionally deviates from its usual form due to the effects intrinsic to semiconductors. Thus, to take one example of $Ga_{1-x}Mn_xAs$, the spin-orbit coupling should be incorporated into the model of exchange interaction from the very beginning, which leads to the presence of directional anisotropies in exchange coupling as well as implies a nondiagonal tensor form of two-spin interaction.[45,47,48] The dependence of coupling energy on the distance between impurities remains oscillatory in sign, which causes spin frustration. The spatial anisotropy is an additional source of orientational frustration[45] for nearest-neighboring spins. This, in turn, produces an imperfect alignment of localized impurity spins in the ordered phase, lowering the saturation magnetization. Different contributions to this mechanism originate from the multiband structure of DMS near the top of the valence band (heavy and light holes). The picture is additionally complicated by the change in the hole localization degree with magnetic ion content (metal-insulator transition). Another issue is the effect of an applied magnetic field on the band structure of the semiconductor and, thus, on the exchange coupling.[49]

The choice of equal concentration of charge carriers and impurity ions is inspired by the fact that such a regime may be reached, for example, in DMS samples, like the above mentioned $Ga_{1-x}Mn_xAs$, as a result of annealing.[50] However, in the general case of real DMS samples, the importance of the interstitial impurities should be noticed. These interstitial ions exhibit different magnetic properties and yield the free-carrier concentrations not equal to the site impurity concentration.

It could be useful to make some comparison of our approach to the correlated disorder and the method used by Meilikhov.[20] In contrast to that study, we do not restrict ourselves to the limit of very low impurity concentration. Thus, we take into consideration the specific lattice by summing the appropriate quantities over discrete fcc lattice sites instead of treating the sample as a continuous medium and

performing integration, which would leave only the dependence on the dimensionality. As a consequence, we do not characterize the impurity correlations by an arbitrary function of the continuous distance (which only vanishes inside the restricted volume between the given site and the nearest neighbors), but we introduce the Warren–Cowley parameters instead. It is worth noticing that the experimentally observed correlations in alloys often change sign while moving between the subsequent coordination zones, which is incorporated in our assumption that the WC parameters are nonzero only for nearest neighbors and next-nearest neighbors of a given site. On the contrary, the correlation function adopted by Meilikhov is rather long ranged and monotonous. We also analyze a more general case, allowing both attractive and repulsive interactions between the ions. In our study, the physically allowed range of the α parameters plays an important role and depends essentially on the lattice geometry.

In our approach, we assume an averaged molecular field acting on each spin in the system, not introducing the distribution of fields, which is a good approximation when the interaction is long ranged (even if exponentially damped). As one of our main goals is to construct the ground-state phase diagram for our model, we believe that when $T \rightarrow 0$, even the relatively weak components of the molecular field coming from rather distant magnetic moments may contribute to the creation of an ordered ground state. Here, it may be useful to recall the experimental findings of Fedorych *et al.*,[51] who stated that the field acting on a Mn spin in $Ga_{1-x}Mn_xAs$ is well averaged and its range is longer than the mean distance between the magnetic impurities, so that a single spin interacts with a significant number of other spins due to an indirect mechanism. As a consequence, an efficient disorder averaging takes place in the metalliclike regime of the delocalized charge carriers. The molecular field we use [Eqs. (21) and (22)] includes an averaged effect of the clustering by virtue of its dependence on WC parameters.

IV. CONCLUSION

The magnetic phase diagrams for the diluted fcc lattice with modified RKKY interaction have been studied, with SRO parameter and external magnetic field taken into account. The formalism necessary for structural averaging in the pair approximation has been presented in the Appendix. As a result, the physical range of the Warren–Cowley parameter has been established. In the theoretical part, the general statistical-thermodynamical method has been presented. On the basis of the above formalism, the phase diagrams and other magnetic properties can be studied in the external field H^z.

A rich ground-state phase diagram was found for the presented model. Both the external field H^z and other Hamiltonian parameters (J^{AF} and λ) have a significant effect on the diagram, especially in a small concentration region. In particular, the external field favors the F phase at the expense of other orderings. Among others, the P phase is found in the ground state, albeit in a very confined region. The numerical calculations show also that the SRO parameter α_1 has a remarkable influence on the phase diagrams, both in the ground state and for the temperature dependency, especially for low n. Both positive and negative structural ordering parameters have been considered. All the phase boundaries presented in the ground state correspond to the discontinuous phase transitions. The temperature phase diagrams contain the vertical phase boundaries, which also represent first-order phase transitions for $T \geqslant 0$. The diluted system with RKKY interaction is mostly a very frustrated one, and the frustration parameter f depends both on the SRO and the parameters of modified interaction. The inverse correlation between the degree of frustration and the critical temperature has been established. The presented method incorporates the Warren–Cowley parameter into the magnetic model, which can be easily extended to other systems, where the structural clustering can play a role in magnetic phenomena. A comparison of the results with those for the virtual crystal approximation can be easily made by assuming $\alpha_1 = 0$.

Although our aim was to study a simple and transparent model of diluted magnets inspired by DMS systems, we note that some qualitative features commonly known from the experiment seem to be present in the results. These involve the existence of a maximum of the Curie temperature for an impurity concentration below ~ 0.1, the presence of a ferromagnetically ordered state in a limited range of low impurity concentrations as well as a rather high frustration level.

The studies presented here, owing to their simplicity and exact results for the ground-state, can be regarded as a point for comparison when more advanced models are considered. In particular, a non-Ising Hamiltonian resulting from the spin-orbit coupling for the holes[45,47,48] and describing a more realistic case for some DMS systems can be taken into account. Nevertheless, for more complicated models, the approximate approach seems unavoidable, even for the ground state.

ACKNOWLEDGMENT

This work was supported by the European Social Fund and Budget of State implemented under the Integrated Regional Operational Program, Action 2.6, Project GRRI-D.

APPENDIX: ATOMIC SHORT-RANGE ORDER IN DILUTED SYSTEMS

We consider a system of localized spins on the crystalline lattice. In such a system, the spin dilution can be conveniently described by means of site occupation operators ξ_i (Ref. 38) for each site, possessing the eigenvalues 0 (the corresponding ith site is empty) and 1 (the ith site is occupied by the magnetic impurity ion). The probability distribution of the eigenvalues of the single-site occupation operator is as follows (see, for example, Ref. 52):

$$p(\xi_i) = n\delta(\xi_i - 1) + (1 - n)\delta(\xi_i), \tag{A1}$$

where $\delta(\xi_i - 1)$ and $\delta(\xi_i)$ are the Kronecker deltas. It can be verified that $\Sigma_{\xi_i=0,1} p(\xi_i) = 1$, thus the distribution is normalized.

The configurational average of the operator ξ_i equals

$$\langle \xi_i \rangle_r = \sum_{\xi_i=0,1} \xi_i p(\xi_i) = n, \tag{A2}$$

so that it is the occupation probability for a single site (i.e., average number of magnetic impurities per site). The average $\langle \xi_i \rangle_r$ is independent of the ith site location, which comes from the fact that the distribution (A1) is valid for the whole sample.

Let us consider a general probability distribution of the occupation of a pair of sites i and j:

$$p(\xi_i, \xi_j) = p_{ij}^{00} \delta(\xi_i) \delta(\xi_j) + p_{ij}^{01} \delta(\xi_i) \delta(\xi_j - 1) + p_{ij}^{10} \delta(\xi_i - 1) \delta(\xi_j) + p_{ij}^{11} \delta(\xi_i - 1) \delta(\xi_j - 1). \tag{A3}$$

The number p_{ij}^{AB} is the probability of the event AB $(A,B=0,1)$ for the pair of lattice sites i and j.

The normalization requires

$$p_{ij}^{00} + p_{ij}^{01} + p_{ij}^{10} + p_{ij}^{11} = 1. \tag{A4}$$

The simplest approach to the description of the diluted system, so-called virtual crystal approximation (VCA), relies on the assumption that the impurity ions are distributed randomly in the lattice sites, thus they are uncorrelated. Then the occupations of the specified sites are statistically independent events and the probability distribution (A3) takes a product form $p(\xi_i, \xi_j) = p(\xi_i) p(\xi_j)$, so $p_{ij}^{00} = (1-n)^2$, $p_{ij}^{01} = p_{ij}^{10} = n(1-n)$, and $p_{ij}^{11} = n^2$. In such a situation, the only parameter describing the distribution of magnetic impurities is n.

However, VCA does not include the possible SRO in the diluted system, which takes place when the occupations of specific sites are not independent events, implying then that $p(\xi_i, \xi_j) \neq p(\xi_i) p(\xi_j)$. In particular, when $p(\xi_i, \xi_j) > p(\xi_i) p(\xi_j)$, we deal with clustering. The existence of SRO stems from the interactions between the impurity ions (especially the Coulombic ones).

The general form of the two-site probability distribution (A3) must be reducible to one-site distributions as follows:

$$\sum_{\xi_i=0,1} p(\xi_i, \xi_j) = p(\xi_j), \tag{A5a}$$

$$\sum_{\xi_j=0,1} p(\xi_i, \xi_j) = p(\xi_i). \tag{A5b}$$

The above conditions, together with Eq. (A1), yield

$$p_{ij}^{00} + p_{ij}^{10} = n,$$

$$p_{ij}^{01} + p_{ij}^{11} = 1 - n, \tag{A6a}$$

$$p_{ij}^{00} + p_{ij}^{01} = n,$$

$$p_{ij}^{10} + p_{ij}^{11} = 1 - n. \tag{A6b}$$

Using Eq. (A4), we obtain

$$p_{ij}^{00} = 1 - 2n + p_{ij}^{11}, \quad p_{ij}^{01} = p_{ij}^{10} = n - p_{ij}^{11}. \tag{A7}$$

Thus, the general two-site probability distribution can be parametrized independently by n and p_{ij}^{11}.

The average of the pair occupation operator reads

$$\langle \xi_i \xi_j \rangle_r = \sum_{\xi_i, \xi_j=0,1} \xi_i \xi_j p(\xi_i, \xi_j) = p_{ij}^{11}, \tag{A8}$$

thus it equals the probability of occupation of both sites i and j simultaneously. For VCA, the average factorizes, $\langle \xi_i \xi_j \rangle_r = \langle \xi_i \rangle_r \langle \xi_j \rangle_r$, due to the product form of $p(\xi_i, \xi_j)$.

Let us write the site occupation operator as follows:

$$\xi_i = \langle \xi_i \rangle_r + \delta \xi_i, \tag{A9}$$

where $\langle \delta \xi_i \rangle_r = 0$ to fulfill Eq. (A2). Thus, in a general case we obtain

$$\langle \xi_i \xi_j \rangle_r = n^2 + \langle \delta \xi_i \delta \xi_j \rangle_r. \tag{A10}$$

Let us denote $\langle \delta \xi_i \delta \xi_j \rangle_r = \Delta_k$. The above expression describes isotropic correlations; i.e., the value $\langle \xi_i \xi_j \rangle_r$ depends solely on the distance r_k between sites i and j (the jth site lies on the kth coordination zone of the ith site). In particular, we have $\Delta_k = 0$ in the absence of SRO for VCA. In the above notation, the probabilities are the following:

$$p_{ij}^{00} = 1 - 2n + n^2 + \Delta_k, \quad p_{ij}^{01} = p_{ij}^{10} = n - n^2 - \Delta_k,$$

$$p_{ij}^{11} = n^2 + \Delta_k. \tag{A11}$$

One can also write the conditional probabilities as follows:

$$p_{ij}^{0|1} = \frac{n - n^2 - \Delta_k}{1 - n}, \quad p_{ij}^{0|0} = 1 - \frac{n - n^2 - \Delta_k}{1 - n},$$

$$p_{ij}^{1|1} = \frac{n^2 + \Delta_k}{n}, \quad p_{ij}^{1|0} = 1 - \frac{n^2 + \Delta_k}{n}, \tag{A12}$$

where $p_{ij}^{A|B}$ is the conditional probability of an event $B=0,1$ for the site j under the condition that an event $A=0,1$ occurred for the site i. It can be verified that the above probabilities obey the Bayes theorem as well as the complete probability theorem.

The possible physical range of Δ_k follows from the interpretation of p_{ij}^{00}, p_{ij}^{01}, p_{ij}^{10}, and p_{ij}^{11} as probabilities, obeying $0 \leq p_{ij}^{AB} \leq 1$. Using Eq. (A11), we arrive at the following set of inequalities:

$$-n^2 + 2n - 1 \leq \Delta_k \leq -n^2 + 2n,$$

$$-n^2 + n - 1 \leq \Delta_k \leq -n^2 + n,$$

$$-n^2 \leq \Delta_k \leq -n^2 + 1, \tag{A13}$$

which must hold for every k.

There exists another condition to impose on the parameters Δ_k. Let us consider the operator of the total number of occupied pairs, $\frac{1}{2}\Sigma_{i,j \neq i} \xi_i \xi_j$, with the following average:

$$\frac{1}{2} \sum_{i,j \neq i} \langle \xi_i \xi_j \rangle_r = \frac{1}{2} N \sum_k z_k (n^2 + \Delta_k). \tag{A14}$$

In the equation above, z_k denotes the number of lattice sites on the kth coordination zone. If we deal with a constant number of impurity ions in the lattice, then the total number of occupied pairs is also constant and does not depend on the

SRO existence. As mentioned above, $\Delta_k \equiv 0$ in the absence of SRO. Therefore, by comparison of Eq. (A14) taken for the absence of SRO and for an arbitrary choice of impurity correlations, we obtain a constraint

$$\sum_k z_k \Delta_k = 0. \tag{A15}$$

Let us restrict ourselves to the situation when SRO is limited to nearest and next-nearest neighbors of each site, i.e., when $\Delta_1 \neq 0$ and $\Delta_2 \neq 0$, while $\Delta_k = 0$ for $k > 2$. Note that the constraint (A15) excludes the possibility that only a single value of Δ_k, for instance, for NN, is nonzero. Therefore, the situation we selected involves a minimal number of Δ_k parameters. Since the constraint gives $\Delta_2 = -(z_1/z_2)\Delta_1$, the distribution of impurities is then described by two independent numbers n and Δ_1.

Writing the inequalities (A13) for Δ_1 and for Δ_2 expressed by Δ_1, we arrive at the allowed range of the parameter Δ_1, which has to fulfill the following 12 inequalities:

$$-n^2 + 2n - 1 \leqslant \Delta_1 \leqslant -n^2 + 2n,$$

$$-n^2 + n - 1 \leqslant \Delta_1 \leqslant -n^2 + n,$$

$$-n^2 \leqslant \Delta_1 \leqslant -n^2 + 1,$$

$$\frac{z_2}{z_1}(n^2 - 2n) \leqslant \Delta_1 \leqslant \frac{z_2}{z_1}(n^2 - 2n + 1),$$

$$\frac{z_2}{z_1}(n^2 - n) \leqslant \Delta_1 \leqslant \frac{z_2}{z_1}(n^2 - n + 1),$$

$$\frac{z_2}{z_1}(n^2 - 1) \leqslant \Delta_1 \leqslant \frac{z_2}{z_1}n^2. \tag{A16}$$

The existence of SRO in diluted systems can also be conveniently described by means of the WC parameters α_{ij},[39] defined as follows:

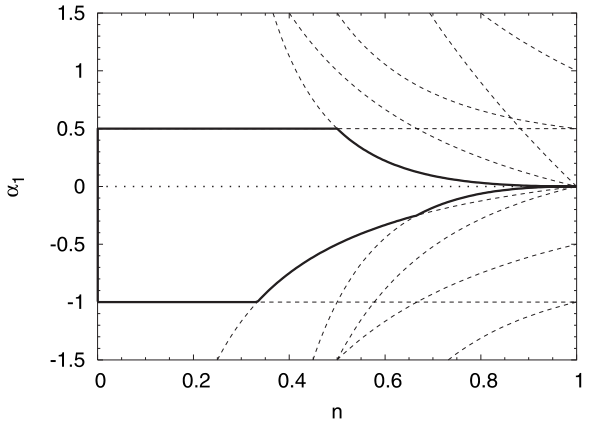

FIG. 9. The allowed range of Warren–Cowley parameter for the first coordination zone of the fcc lattice. The dashed lines (12 in total) are the limits obtained from the inequalities (A16). The thick solid line encloses the allowed range of α_1 for various n. The dotted line for $\alpha_1 = 0$ corresponds to vanishing SRO.

$$\alpha_{ij} = \frac{\langle \xi_i \xi_j \rangle_r - \langle \xi_i \rangle_r \langle \xi_j \rangle_r}{\langle \xi_i \rangle_r \langle \xi_j \rangle_r}. \tag{A17}$$

These parameters can be equivalently given in the form $\alpha_{ij} = -(1 - p_{ij}^{1|1}/n)$, where $p_{ij}^{1|1} = p_{ij}^{11}/n$ is a conditional probability of occupying the jth site if the ith site is occupied.

In our notation, the WC parameter for the kth coordination zone is given by

$$\alpha_k = \Delta_k / n^2 \tag{A18}$$

and the configurational average of pair occupation operator reads

$$\langle \xi_i \xi_j \rangle_r = n^2(1 + \alpha_k). \tag{A19}$$

The allowed range of WC parameter α_1 values for Δ_1 fulfilling the inequalities (A16) for a fcc lattice is presented in Fig. 9, where it is bounded by thick solid lines. In this range, the physically possible correlations are given by Eq. (A19). For other lattices characterized by specific sets of z_k numbers, the range of WC parameter requires separate calculations based on the inequalities (A16).

*kszalowski@uni.lodz.pl

[1] D. C. Mattis, *The Theory of Magnetism II* (Springer-Verlag, Berlin, 1985).
[2] J. Jensen and A. R. Mackintosh, *Rare Earth Magnetism: Structures and Excitations* (Oxford University Press, Oxford, 1991).
[3] H. Ohno, Science **281**, 951 (1998).
[4] T. Dietl, A. Haury, and Y. M. d'Aubigné, Phys. Rev. B **55**, R3347 (1997).
[5] T. Jungwirth *et al.*, Phys. Rev. B **76**, 125206 (2007).
[6] T. Jungwirth, J. Sinova, J. Mašek, J. Kučera, and A. H. MacDonald, Rev. Mod. Phys. **78**, 809 (2006).
[7] P. G. de Gennes, J. Phys. Radium **23**, 630 (1962).
[8] P. F. de Châtel, J. Magn. Magn. Mater. **23**, 28 (1981).
[9] D. C. Mattis, *The Theory of Magnetism I* (Springer-Verlag, Berlin, 1981).
[10] T. Dietl, H. Ohno, F. Matsukura, J. Cibert, and D. Ferrand, Science **287**, 1019 (2000).
[11] S. Das Sarma, E. H. Hwang, and D. J. Priour, Jr., Phys. Rev. B **70**, 161203(R) (2004).
[12] D. J. Priour, Jr., E. H. Hwang, and S. Das Sarma, Phys. Rev. Lett. **92**, 117201 (2004).
[13] D. J. Priour, Jr. and S. Das Sarma, Phys. Rev. Lett. **97**, 127201 (2006).
[14] D. J. Priour, Jr. and S. Das Sarma, Phys. Rev. B **73**, 165203 (2006).
[15] R. Bouzerar, G. Bouzerar, and T. Ziman, Phys. Rev. B **73**,

024411 (2006).
[16] M. J. Calderón and S. Das Sarma, Phys. Rev. B **75**, 235203 (2007).
[17] M. Mayr, G. Alvarez, and E. Dagotto, Phys. Rev. B **65**, 241202(R) (2002); M. P. Kennett, M. Berciu, and R. N. Bhatt, *ibid.* **66**, 045207 (2002); M. J. Calderón, G. Gómez-Santos, and L. Brey, *ibid.* **66**, 075218 (2002).
[18] C. Timm, J. Phys.: Condens. Matter **15**, R1865 (2003).
[19] S. J. Potashnik, K. C. Ku, S. H. Chun, J. J. Berry, N. Samarth, and P. Schiffer, Appl. Phys. Lett. **79**, 1495 (2001).
[20] E. Z. Meilikhov, Phys. Rev. B **75**, 045204 (2007).
[21] G. Bouzerar, T. Ziman, and J. Kudrnovský, Appl. Phys. Lett. **85**, 4941 (2004).
[22] V. Drchal, J. Kudrnovský, I. Turek, F. Máca, and P. Weinberger, Philos. Mag. **84**, 1889 (2004).
[23] J. Kudrnovský, V. Drchal, G. Bouzerar, and R. Bouzerar, Phase Transitions **80**, 333 (2007).
[24] H. Raebiger, A. Ayuela, and J. von Boehm, Phys. Rev. B **72**, 014465 (2005).
[25] M. Berciu and R. N. Bhatt, Phys. Rev. Lett. **87**, 107203 (2001).
[26] J. L. Xu, M. van Schilfgaarde, and G. D. Samolyuk, Phys. Rev. Lett. **94**, 097201 (2005).
[27] G. Tang and W. Nolting, Phys. Status Solidi B **244**, 735 (2007).
[28] A. Franceschetti, S. V. Barabash, J. Osorio, A. Zunger, and M. van Schilfgaarde, Phys. Rev. B **74**, 241303(R) (2006).
[29] L. M. Sandratskii and P. Bruno, J. Phys.: Condens. Matter **16**, L523 (2004).
[30] A. Franceschetti, A. Zunger, and M. van Schilfgaarde, J. Phys.: Condens. Matter **19**, 242203 (2007).
[31] G. Bouzerar and J. Kudrnovský, Europhys. Lett. **69**, 812 (2005).
[32] P. W. Anderson, Phys. Rev. **79**, 705 (1950).
[33] J. S. Smart, Phys. Rev. **86**, 968 (1952).
[34] A. H. Morrish, *The Physical Principles of Magnetism* (Wiley, New York, 1965).
[35] T. Balcerzak, J. W. Tucker, A. Bobák, and M. Jaščur, Czech. J. Phys. **54**, D643 (2004).
[36] T. Balcerzak, Phys. Status Solidi C **3**, 212 (2006).
[37] K. Szałowski and T. Balcerzak, Acta Phys. Pol. A **113**, 421 (2008).
[38] S. F. Edwards and J. M. Loveluck, J. Phys. C **3**, S261 (1970).
[39] J. M. Cowley, J. Appl. Phys. **21**, 24 (1950); Phys. Rev. **77**, 669 (1950).
[40] M. A. Ruderman and C. Kittel, Phys. Rev. **96**, 99 (1954); T. Kasuya, Prog. Theor. Phys. **16**, 45 (1956); K. Yosida, Phys. Rev. **106**, 893 (1957).
[41] J. Kudrnovský, I. Turek, V. Drchal, F. Máca, P. Weinberger, and P. Bruno, Phys. Rev. B **69**, 115208 (2004).
[42] J. Okabayashi, A. Kimura, O. Rader, T. Mizokawa, A. Fujimori, T. Hayashi, and M. Tanaka, Phys. Rev. B **58**, R4211 (1998).
[43] H. Ohno, A. Shen, F. Matsukura, A. Oiwa, A. Endo, S. Katsumoto, and Y. Iye, Appl. Phys. Lett. **69**, 363 (1996).
[44] H. Ohno and F. Matsukura, Solid State Commun. **117**, 179 (2001).
[45] G. Zaránd and B. Jankó, Phys. Rev. Lett. **89**, 047201 (2002).
[46] C. Zhou, M. P. Kennett, X. Wan, M. Berciu, and R. N. Bhatt, Phys. Rev. B **69**, 144419 (2004).
[47] G. A. Fiete, G. Zaránd, K. Damle, and C. P. Moca, Phys. Rev. B **72**, 045212 (2005); G. A. Fiete, G. Zaránd, B. Jankó, P. Redliński, and C. P. Moca, *ibid.* **71**, 115202 (2005); G. A. Fiete, G. Zaránd, and K. Damle, Phys. Rev. Lett. **91**, 097202 (2003).
[48] C. Timm and A. H. MacDonald, Phys. Rev. B **71**, 155206 (2005).
[49] C. H. Ziener, S. Glutsch, and F. Bechstedt, Phys. Rev. B **70**, 075205 (2004).
[50] T. Jungwirth *et al.*, Phys. Rev. B **72**, 165204 (2005).
[51] O. M. Fedorych, Z. Wilamowski, M. Potemski, M. Byszewski, and J. Sadowski, Acta Phys. Pol. A **103**, 607 (2003); Semicond. Sci. Technol. **19**, S492 (2004).
[52] M. F. Thorpe and D. Beeman, Phys. Rev. B **14**, 188 (1976); O. F. de Alcantara Bonfim and I. P. Fittipaldi, Phys. Lett. **98A**, 199 (1983).